B-meson semileptonic decays from highly improved staggered quarks

Andrew Lytle,[a,*] **Carleton DeTar,**[b] **Aida El-Khadra,**[a] **Elvira Gámiz,**[c] **Steven Gottlieb,**[d] **William Jay,**[e] **Andreas Kronfeld,**[f] **Jack Laiho,**[g] **James Simone**[f] **and Alejandro Vaquero**[h]

[a]*Department of Physics and Illinois Center for Advanced Studies of the Universe, University of Illinois, Urbana, Illinois, 61801, USA*

[b]*Department of Physics and Astronomy, University of Utah, Salt Lake City, Utah 84112, USA*

[c]*Departamento de Física Teórica y del Cosmos, Universidad de Granada, E-18071, Spain*

[d]*Department of Physics, Indiana University, Bloomington, Indiana 47405, USA*

[e]*Center for Theoretical Physics, Massachusetts Institute of Technology, Cambridge, MA 02139, USA*

[f]*Theory Division, Fermi National Accelerator Laboratory, Batavia, Illinois, 60510, USA*

[g]*Department of Physics, Syracuse University, Syracuse, NY 13244, USA*

[h]*CAPA & Departamento de Física Teórica, Universidad de Zaragoza, 50009 Zaragoza, Spain*

E-mail: atlytle@illinois.edu

We present an update for results on B-meson semileptonic decays using the highly improved staggered quark (HISQ) action for both valence and 2+1+1 sea quarks. The use of the highly improved action, combined with the MILC collaboration's gauge ensembles with lattice spacings down to ~0.03 fm, allows the b quark to be treated with the same discretization as the lighter quarks. The talk will focus on updated results for $B_{(s)} \to D_{(s)}$, $B_{(s)} \to K$ scalar and vector form factors.

---

*Speaker

arXiv:2403.03959v2 [hep-lat] 18 Mar 2024

1. Introduction

Lattice QCD calculations of meson-decay form factors are crucial inputs for high-precision tests of the Standard Model (SM) of particle physics. Combined with the corresponding experimentally measured decay rates, the lattice determinations of hadronic flavor-changing matrix elements allow for independent determinations of CKM matrix elements, enabling precision tests of the SM. Lattice form-factor data also give shape information, and pure SM predictions for quantities such as R-ratios.

Thanks to ongoing experimental programs for heavy flavor physics including Belle II, BES III, and those at the LHC, we expect new measurements for many different observables and decay channels with increasing precision in the coming years. Improvements on the SM theory side are therefore well motivated and timely, and will enable sharper tests of the SM, provided theory uncertainties are quantified at a commensurate level as experiment. Some current few-sigma discrepancies (collectively referred to as B-anomalies) may be hints for new physics, (For recent discussions from a lattice perspective, see, e.g., Refs. [1–5].) There are also long-standing differences in inclusive and exclusive extractions of the CKM elements $|V_{ub}|$ and $|V_{cb}|$, which should be resolved. Improved theoretical calculations of B-semileptonic decays will bear directly both on exclusive/inclusive discrepancies, and interpreting B-anomalies. Here we provide a status update of the FNAL-MILC collaboration's calculations of semileptonic $B_{(s)}$-meson decay form factors using the highly improved staggered quark (HISQ) action.

2. Calculation overview

Some of the details of our calculation have been reported previously in Refs. [6, 7]. Here we review the basics and highlight updates from previous reports. Our calculation uses ensembles generated by the MILC Collaboration using $N_f = 2 + 1 + 1$ flavors of dynamical sea quarks with the HISQ action [8–10]. We report preliminary results from ensembles with lattice spacings of $a = 0.09$, 0.06, 0.042, and 0.03 fm. At $a = 0.09$ and 0.06 fm we have generated correlator data on ensembles with light sea-quarks at their physical values as well as at $m_l/m_s = 0.1$ and 0.2. At $a = 0.042$ and 0.03 fm we have analyzed ensembles with $m_l \approx 0.2 m_s$ in the sea, and are currently generating 0.042 fm data with physical light quarks in the sea. The strange and charm sea-quark masses are tuned to be close to their physical values, and the valence light- and strange-quark masses are taken to be equal to the corresponding sea-quark masses. The heavy valence quarks range in mass from roughly $0.9 m_c$ to near the lattice cutoff, $am_h \approx 1$. At the finest lattice spacings, this setup allows simulation close to, or in the case of $a = 0.03$ fm directly at, the physical mass of the bottom quark.

To determine the required form factors, we first extract matrix elements from joint correlated fits to two-point and three-point correlation functions. More details of our correlators and fit forms are given in Ref. [6]. A schematic of a generic three point function used in our fits is shown in Fig. 1. As usual for staggered fermions, the correlation functions include smoothly decaying contributions with the desired parity as well as oscillating contributions from states of opposite parity. We fit these correlators varying the number of even and odd states (n, m), checking stability in our final results to these variations.
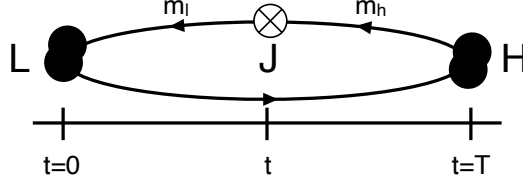
Figure 1: A schematic of the 3pt functions used to determine matrix elements entering Eqs. (1)–(3) The light final state hadron is created with momentum p at the origin. An external current J is inserted at time t. The heavy hadron is destroyed at rest at time T.

All of our results are blinded by a random factor that is common for all three-point functions of a given analysis/decay channel. We will carry the analysis of the blinded form factors all the way through the chiral interpolation and continuum extrapolation, unblinding only when the analysis of systematic errors is complete.

3. Form factors

Having extracted scalar and vector three-point matrix elements from simultaneous fits, we can relate these to decay form factors via

$$f_\parallel = Z_{V^0} \frac{\langle L | V^0 | H \rangle}{\sqrt{2M_H}} \tag{1}$$

$$f_\perp = Z_{V^i} \frac{\langle L | V^i | H \rangle}{\sqrt{2M_H}} \frac{1}{p_L^i} \tag{2}$$

$$f_0 = \frac{m_h - m_\ell}{M_H^2 - M_L^2} \langle L | S | H \rangle . \tag{3}$$

In these expressions, M_H, M_L, p_H^μ, and p_L^μ refer to the mass and four-momentum of the heavy initial (H) and light final state (L) mesons; m_h and m_ℓ refer to the heavy and light input quark masses of the transition current. The final equality relating f_0 to the scalar matrix element follows from partial conservation of the vector current.

In Fig. 2, we show results for the $H_s \to D_s$ scalar form factor f_0 at zero recoil, as a function of the heavy proxy meson mass $M(H_s)$. For this decay involving no light quarks and at zero-recoil, the data itself are very precise. On our finest ensembles $a = 0.042$ fm and $a = 0.03$ fm, we have data points near to (and for $a = 0.03$ fm beyond) the physical B_s mass, indicated by a vertical dotted line in the figure. For the $a = 0.09$ fm and $a = 0.06$ fm data, we have results with two different light-quark masses in the sea. The extremely weak sea-quark mass dependence is evident here. We can perform a simple fit to the data, modeling the physical dependence as a polynomial in $1/M_{H_s}$ and discretization artifacts as a polynomial in $(am_h)^2$,

$$f_0(q_{\max}^2)[M_{H_s}, am_h] = \sum_{ij} c_{ij} \left(\frac{1}{M_{H_s}} \right)^i \left(am_h \right)^{2j} \tag{4}$$

to determine the physical result for the $f_0(q_{\max}^2)$ form factor. The continuum result for the form factor as a function of $M(H_s)$ is given by the black dashed line.
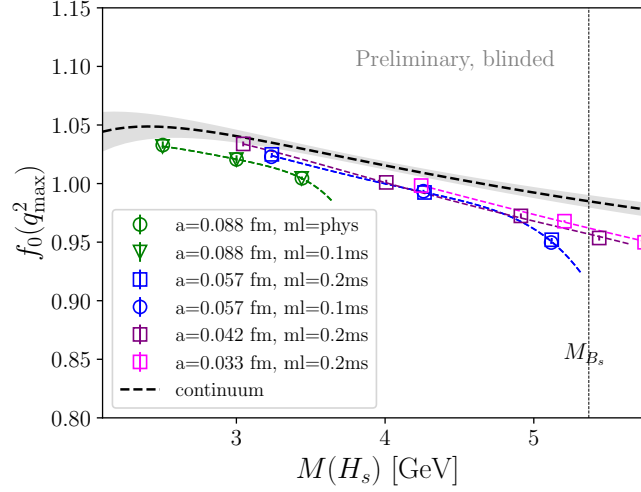
Figure 2: An example continuum fit for the $B_s \to D_s$ decay f_0 form factor, at the zero-recoil ($q^2_{\max}$) point. Here the x axis gives the mass of a proxy H_s meson, the results at the physical B_s mass are marked by the vertical dotted line. The symbols give the results from lattice data, while the dotted lines give the results of the fit evaluated for the given ensemble parameters. The black dashed line and gray band give the results of the fit evaluated in the $a \to 0$ limit. Note the data are blinded.

At Lattice 2022, we showed raw data for the $B_s \to D_s$ decay f_0, $f_\parallel$, and $f_\perp$ form factors [6]. Here, we focus on the analogous data relevant for the decay $B_s \to K$, obtained by using $h \to l$ currents instead of the $h \to c$ currents for the former decay. Raw data for these decays are given by the colored symbols in Fig. 4. For this figure, we are displaying only data $m_h \lesssim 3.0 m_c$, and we discuss a preliminary chiral and continuum fit to the data in the next section. We observe good precision in the data, especially at lower recoil, though overall the data is noisier than for $B_s \to D_s$ on account of the light quark propagator.

4. Vector current normalization

We renormalize our vector currents based on partial conservation of the vector current (PCVC). Applied to our lattice matrix elements, PCVC implies the relation

$$Z_{V^4}(M_H - E_L)\langle L|V^4|H\rangle + Z_{V^i}\mathbf{q}\cdot\langle L|\mathbf{V}|H\rangle = (m_h - m_l)\langle L|S|H\rangle. \tag{5}$$

In the proceeding [6], we applied this relation in a two-step process to determine the Z-factors Z_{V^4} and Z_{V^i} for the local-temporal and one-link spatial vector currents, respectively. First zero-momentum correlators were used to determine Z_{V^4}, and then this was used with correlators with a chosen non-zero momentum to extract Z_{V^i}. Although this is straightforward, it requires a specific choice of momentum, and does not leverage information from correlators with other momenta. Here, we instead follow the strategy of Ref. [11], and fit Eq. (5) using all momenta values to find best-fit values for the Z-factors. Sample results of this exercise are shown in Fig. 3 where we display Z_{V_4} values for the heavy-to-light current relevant for $B_s \to K$. We observe decent precision, in most cases well below 1%, for the Z-factors. We note that the precision of the determination tends to decrease for heavier physical mass values.
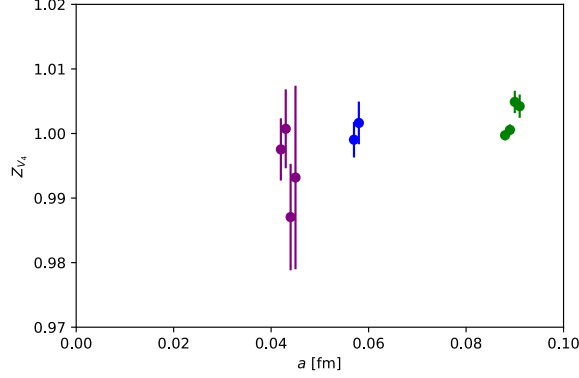
Figure 3: Z_{V_4} values for the heavy-light local temporal current, obtained by fitting Eq. (5), as described in the text. Results are shown for several heavy quark mass values on each ensemble. The points within each ensemble, corresponding to different heavy mass values, are offset slightly, with mass values increasing from left to right. We observe decent precision in the data, which decreases somewhat as the H_s meson mass increases.

5. Combined chiral-continuum fits

We can perform a chiral and continuum fit to the data, shown in Fig. 4. We base our preliminary fits on hard $SU(2)\,\chi$PT, used in the FNAL-MILC analysis of D-decays [11]. Note that the dataset we consider here can be considered as an extension of that dataset, including quark masses approaching the physical bottom mass. In order to simultaneously fit data across a range of m_h values, we will extend the chiral forms used in Ref. [11] to include additional terms in an HQET-inspired expansion.

The chiral expressions from [11] take the schematic form

$$f_{0,\parallel,\perp}(E) = \frac{c_0}{E + \Delta}(1 + \cdots + c_H \chi_{H_s} + \cdots) \tag{6}$$

$$\Delta = \frac{M_{D^*}^2 - M_{D_s}^2 - M_K^2}{2 M_{D_s}}, \qquad \chi_{H_s} = \frac{\Lambda_{\text{HQET}}}{M_{H_s}} - \frac{\Lambda_{\text{HQET}}}{M_{D_s}^{\text{PDG}}} \tag{7}$$

where we have broken out explicitly pieces of the expression that are modified. We model the physical dependence of the coefficient c_0, similar to Ref. [10], and the splitting term (treating the $D^* - D_s$ splitting to a first approximation as independent of heavy quark mass), while the mistuning term χ_{H_s} is shifted to be around the physical target final state, which we take to be at $m_h = 3m_c$. As we refine the fits we will include the complete datasets at finer lattice spacings and shift this to $m_h = m_b$. The modifications to the fit function are thus given by

$$c_0 \to c_0 + c_1 \frac{\Lambda_{\text{HQET}}}{M_{H_s}} + \cdots, \quad \Delta \to \frac{M_{D^*}^2 - M_{D_s}^2 - M_K^2}{2 M_{H_s}} \text{ (1st order)}, \tag{8}$$

$$\chi_{H_s} = \frac{\Lambda_{\text{HQET}}}{M_{H_s}} - \frac{\Lambda_{\text{HQET}}}{M_{H_s}^{3m_c}}. \tag{9}$$

The fit results evaluated at the ensemble parameters are given as colored lines matching the symbol colors in Fig. 4. The continuum results, evaluated at $m_h = 3m_c$, are shown as a black curve, and
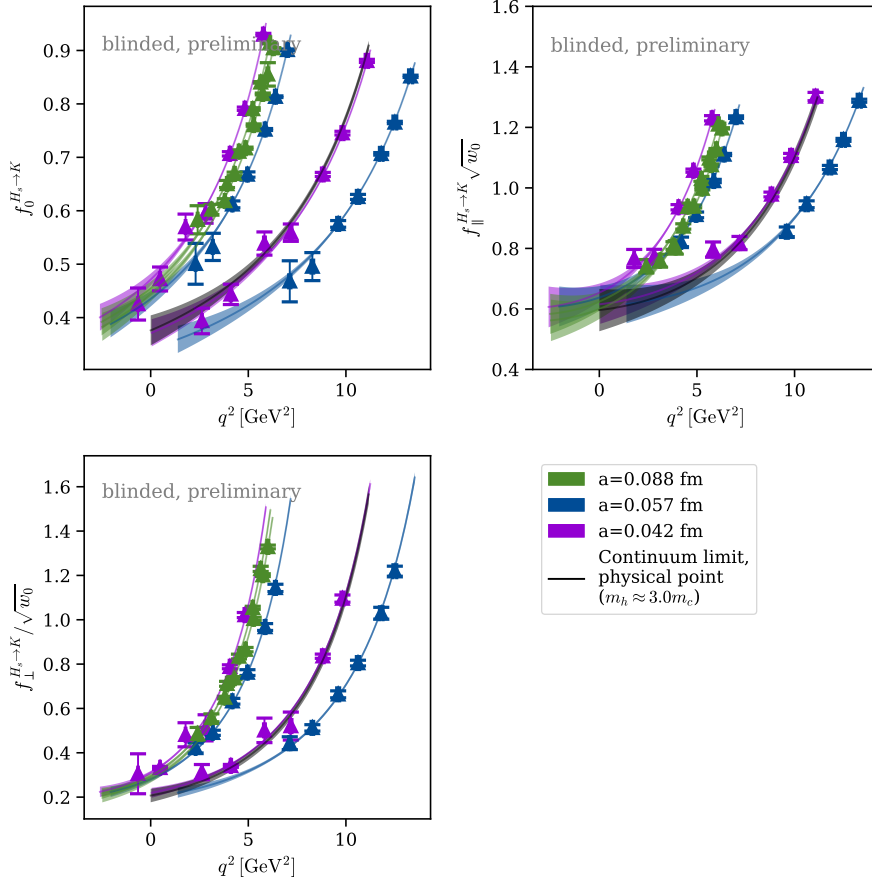
Figure 4: Example, preliminary chiral fits for the $H_s \to K$ semileptonic decay, including form factors f_0, $f_{\parallel}$, and $f_{\perp}$. The data shown here include heavy proxy masses of $m_h \approx 2m_c$ for 0.09 fm data (with different symbols denoting two different sets of sea masses, $m_l = 0.1m_s$, phys), $m_h \approx 2.2, 3.3m_c$ for 0.06 fm data, and $m_h \approx 2, 3m_c$ for 0.042 fm data. For this preliminary fit, we took the physical heavy mass to be $m_h = 3m_c$, and the continuum curve is given as a black line, nearly overlapping with $3m_c$ data computed at our finest lattice spacing of 0.042 fm.

track fairly closely the $3 m_c$ data at $a = 0.042$ fm, indicating that discretization and chiral effects are fairly mild. The fits return $\chi^2/\mathrm{dof} = 0.92, 1.79, 0.75$ for $f_0, f_{\parallel}, f_{\perp}$.

6. Summary

In this proceeding we provided a status update on the FNAL-MILC B-meson semileptonic decay calculations using HISQ quarks. We have extended our datasets to the $a = 0.03$ fm ensemble with $m_l = 0.2m_s$ light quarks in the sea. This lattice spacing can comfortably accommodate the b quark, and our heaviest simulation masses straddle the b mass input parameter. Calculations on an ensemble with physical quarks and $a = 0.042$ fm are underway, and preliminary results on this ensemble should be expected in the next year. Combined with results from varying sea masses on

$a = 0.09$ and $a = 0.06$ fm ensembles, this should ensure good control over chiral effects in our final results.

We presented new, blinded results relevant for the $B_s \rightarrow K$ decay, which may be used to extract $|V_{ub}|$. We presented our strategy to build on the chiral-continuum strategy used in D-decays, discussing preliminary chiral-continuum fits of this data. We also presented first results for the vector-current renormalizations relevant for this decay, using a fitting strategy that leverages the complete data set. We found values for Z_{V_4} that are close to 1, and generally have sub-percent precision, although the precision decreases as heavier masses are considered.

7. Acknowledgments

References

[1] P. A. Boyle, B. Chakraborty, C. T. H. Davies, T. DeGrand, C. DeTar, L. Del Debbio, A. X. El-Khadra, F. Erben, J. M. Flynn and E. Gámiz, *et al.* [arXiv:2205.15373 [hep-lat]].

[2] A. S. Kronfeld *et al.* [USQCD], [arXiv:2207.07641 [hep-lat]].

[3] Z. Davoudi, E. T. Neil, C. W. Bauer, T. Bhattacharya, T. Blum, P. Boyle, R. C. Brower, S. Catterall, N. H. Christ and V. Cirigliano, *et al.* [arXiv:2209.10758 [hep-lat]].

[4] J. T. Tsang and M. Della Morte, doi:10.1140/epjs/s11734-023-01011-3 [arXiv:2310.02705 [hep-lat]].

[5] A. Vaquero, PoS **LATTICE2022**, 250 (2022) [arXiv:2212.10217 [hep-lat]].

[6] A. Lytle *et al.* [Fermilab Lattice and MILC,], PoS **LATTICE2022**, 418 (2023) doi:10.22323/1.430.0418 [arXiv:2301.09229 [hep-lat]].

[7] W. I. Jay *et al.* [Fermilab Lattice and MILC], PoS **LATTICE2021**, 109 (2022) doi:10.22323/1.396.0109 [arXiv:2111.05184 [hep-lat]].

[8] A. Bazavov *et al.* [MILC], Phys. Rev. D **82**, 074501 (2010) doi:10.1103/PhysRevD.82.074501 [arXiv:1004.0342 [hep-lat]].

[9] A. Bazavov *et al.* [MILC], Phys. Rev. D **87**, no.5, 054505 (2013) doi:10.1103/PhysRevD.87.054505 [arXiv:1212.4768 [hep-lat]].

[10] A. Bazavov, C. Bernard, N. Brown, C. DeTar, A. X. El-Khadra, E. Gámiz, S. Gottlieb, U. M. Heller, J. Komijani and A. S. Kronfeld, *et al.* Phys. Rev. D **98**, no.7, 074512 (2018) doi:10.1103/PhysRevD.98.074512 [arXiv:1712.09262 [hep-lat]].

[11] A. Bazavov *et al.* [Fermilab Lattice and MILC], [arXiv:2212.12648 [hep-lat]].

[12] D. Stanzione, J. West, R.T. Evans, T. Minard, O. Ghattas, and D.K. Panda. In Practice and Experience in Advanced Research Computing (PEARC 2020). July 26–30, 2020, Portland, OR, USA. ACM, New York, NY, USA. doi:10.1145/3311790.3396656

[13] J. Towns, T. Cockerill, M. Dahan, I. Foster, K. Gaither, A. Grimshaw, V. Hazlewood, S. Lathrop, D. Lifka, G.D. Peterson, R. Roskies, J.R. Scott, N. Wilkins-Diehr. "XSEDE: Accelerating Scientific Discovery", Computing in Science & Engineering, vol.16, no. 5, pp. 62-74, Sept.-Oct. 2014, doi:10.1109/MCSE.2014.80